THE JOURNAL OF BIOLOGICAL CHEMISTRY VOL. 281, NO. 13, pp. 8667–8674, March 31, 2006

Structure and Activation Mechanism of the *Drosophila* Initiator Caspase Dronc*[S]

Received for publication, December 12, 2005, and in revised form, January 17, 2006 Published, JBC Papers in Press, January 30, 2006, DOI 10.1074/jbc.M513232200

Nieng Yan[‡], Jun R. Huh[§], Virgil Schirf[¶], Borries Demeler[¶], Bruce A. Hay[§], and Yigong Shi[‡1]

From the [‡]Department of Molecular Biology, Princeton University, Lewis Thomas Laboratory, Princeton, New Jersey 08544, the [§]Division of Biology, California Institute of Technology, Pasadena, California 91125, and the [¶]Department of Biochemistry, The University of Texas Health Science Center at San Antonio, San Antonio, Texas 78229-3900

Activation of an initiator caspase is essential to the execution of apoptosis. The molecular mechanisms by which initiator caspases are activated remain poorly understood. Here we demonstrate that the autocatalytic cleavage of Dronc, an important initiator caspase in *Drosophila*, results in a drastic enhancement of its catalytic activity *in vitro*. The autocleaved Dronc forms a homodimer, whereas the uncleaved Dronc zymogen exists exclusively as a monomer. Thus the autocatalytic cleavage in Dronc induces its stable dimerization, which presumably allows the two adjacent monomers to mutually stabilize their active sites, leading to activation. Crystal structure of a prodomain-deleted Dronc zymogen, determined at 2.5 Å resolution, reveals an unproductive conformation at the active site, which is consistent with the observation that the zymogen remains catalytically inactive. This study revealed insights into mechanism of Dronc activation, and in conjunction with other observations, suggests diverse mechanisms for the activation of initiator caspases.

Caspases, the executioners of cell death, comprise two families, the initiator caspases and the effector caspases (1, 2). Caspase is synthesized as a single-chain zymogen and must undergo an activation process to acquire full catalytic activity. An effector caspase is activated through an intrachain cleavage mediated by a specific initiator caspase. For example, the effector caspase-3 and caspase-7 are processed by the initiator caspase-9 in the intrinsic apoptosis pathway or by the initiator caspase-8 in the extrinsic pathway (2, 3). An initiator caspase, on the other hand, is autoactivated in response to upstream death stimuli. The autoactivation of an initiator caspase is mediated by a specific adaptor protein complex in cells.

The activation mechanism for the effector caspases, as exemplified by caspase-7 (4, 5), is well characterized. Both the zymogen and the active form of caspase-7 are constitutively homodimeric. The active site of one caspase-7 monomer is formed by five surface loops: four from within, named L1, L2, L3, and L4, and the fifth one from the adjacent monomer, named L2′. This structural feature necessitates dimerization for activation of the effector caspases. In the caspase-7 zymogen, the L2′ loop is covalently linked to its N-terminal sequences and is unable to adopt the conformation as required in the activated caspase-7. Consequently, the active site of the caspase-7 zymogen adopts an inactive conformation that does not support catalysis. The intrachain cleavage of caspase-7 zymogen allows the L2′ loop to adopt the correct conformation.

In contrast to effector caspases, the mechanisms of activation for the initiator caspases are poorly understood (6). One of the most intensely studied initiator caspases is caspase-9, the activation of which requires the assembly of the apoptosome, a 1-MDa protein complex composed of Apaf-1, cytochrome *c*, and ATP/dATP (7). Interestingly, the autocleaved caspase-9 remains associated with the apoptosome as an active holoenzyme, and the isolated, cleaved caspase-9 is marginally active (8). The prodomain of caspase-9, which is not cleaved off the caspase unit in the activated enzyme, is primarily responsible for binding to Apaf-1. Both the zymogen and the mature caspase-9 exist as a monomer (9), and the autocatalytic cleavage does not play a critical role in the activation of caspase-9 (10). Despite recent progress (11, 12), the underlying mechanism by which the apoptosome activates caspase-9 remains enigmatic. In contrast to caspase-9, autocatalytic cleavage appears to play an essential role for the activation of caspase-8 (13, 14) and caspase-2 (15). In both cases, the autocatalytic cleavage facilitates the formation of a homodimer for the initiator caspases *in vitro*.

Dronc is the *Drosophila* ortholog of the mammalian initiator caspase-9 and is required for programmed cell death during the normal development of fruit flies (16–18). One important downstream target of Dronc is the effector caspase Drice, an ortholog of mammalian caspase-3. The activation of Dronc in *Drosophila* cells requires Dark/Hac-1/Dapaf-1 (19–21), the ortholog of mammalian Apaf-1. Analogous to caspase-9, the prodomain of Dronc is responsible for interaction with Dark/Hac-1/Dapaf-1.[2] However, in contrast to caspase-9, the prodomain of Dronc is cleaved off the caspase unit in *Drosophila* cells (22), suggesting a different mode of activation. At present, the molecular mechanism by which Dronc is activated remains unknown.

In this study, we report the molecular mechanism for the activation of Dronc cleavage-induced stable dimerization. The Dronc zymogen exists exclusively as a monomer in solution. The intrachain cleavage triggers the preferential formation of a homodimer for the cleaved Dronc, which exhibits a drastically elevated level of catalytic activity when compared with the monomeric zymogen. The crystal structure of a catalytic mutant Dronc in its zymogen form reveals the basis for catalytic dormancy, an unproductive conformation in the active site. Together, these results defined the precise molecular mechanisms by which Dronc is activated.

EXPERIMENTAL PROCEDURES

Protein Preparation—All constructs were generated using a standard PCR-based cloning strategy, and the identities of individual clones were verified through double-stranded plasmid sequencing. All proteins

* This work was supported by grants from the National Institutes of Health. The costs of publication of this article were defrayed in part by the payment of page charges. This article must therefore be hereby marked "*advertisement*" in accordance with 18 U.S.C. Section 1734 solely to indicate this fact.

The atomic coordinates and structure factors (code 2FP3) have been deposited in the Protein Data Bank, Research Collaboratory for Structural Bioinformatics, Rutgers University, New Brunswick, NJ (http://www.rcsb.org/).

[S] The on-line version of this article (available at http://www.jbc.org) contains supplemental text on analytical ultracentrifugation and four supplemental figures.

[1] To whom correspondence should be addressed: Dept. of Molecular Biology, Princeton University, Lewis Thomas Laboratory, Washington Rd., Princeton, NJ 08544. Tel.: 609-258-6071; Fax: 609-258-6730; E-mail: ygshi@princeton.edu.

[2] N. Yan and Y. Shi, unpublished data.

were overexpressed in *Escherichia coli* strain BL21(DE3) either as non-tagged protein using the vector pBB75 or as C-terminal His_6-tagged proteins using pET21b (Novagen). Proteins were purified to homogeneity as described (23).

Crystallization and Data Collection—Crystals of pro-domain-deleted Dronc (residues 136–450, C318A) were obtained by the hanging-drop vapor diffusion method by mixing the complex (10 mg ml^{-1}) with an equal volume of reservoir solution containing 100 mM imidazole, pH 9.0, and 1.1 M ammonium mono-hydrogen phosphate. Cubic-shaped crystals appeared after 5 days and grew to a typical dimension of $0.2 \times 0.2 \times 0.2$ mm^3. They were in the space group I4132 and contained one molecule in each asymmetric unit. The unit cell dimensions are $a = b = c = 165.7$ Å. Selenomethionine-derived proteins were crystallized under a similar condition with the same space group and similar unit cell parameters. Crystals were equilibrated in a cryoprotectant buffer containing well buffer plus 25% glycerol and were flash-frozen in a $^{-}170$ °C nitrogen stream. The native data were collected at the Cornell High Energy Synchrotron Source (CHESS) beamline A1, and seleno-multiple anomalous dispersion data were collected at the CHESS beamline F2 and processed using the software Denzo and Scalepack (24).

Structure Determination—The structure was determined by multiple anomalous dispersion using SOLVE (25). Seven selenium atoms per asymmetric unit were located. These selenium positions were further refined using MLPHARE (26). A model was built using O (27) and refined at 2.5 Å resolution using CNS (28).

Gel Filtration Assay—Individual recombinant proteins were purified to more than 95% homogeneity and incubated in assay buffer (25 mM Tris, pH 8.0, 150 mM NaCl, and 2 mM dithiothreitol) for 10 min at 4 °C. 0.5 ml of the protein mixture was subjected to gel filtration analysis (Superdex 200, Amersham Biosciences) for each run. Samples taken from relevant fractions were applied to SDS-polyacrylamide gel electrophoresis (SDS-PAGE) and visualized by Coomassie Blue staining.

Dronc Activity Assay—Reactions were carried out at 22 °C in an assay buffer containing 25 mM HEPES, pH 7.5, 150 mM NaCl, and 2 mM dithiothreitol. Catalytically inactive DrICE zymogen (C196A) was used as the substrate at a concentration of ~100 μM. Mature Dronc and catalytically active but non-cleavable Dronc zymogen (E352A) were purified to homogeneity and used in each reaction at 100 nM. Reaction samples were taken out at the indicated time points and applied to SDS-PAGE followed by Coomassie Blue staining. Similar results were obtained under pH 6.8 and pH 8.0 as well as a variety of other ionic strength conditions.

Drosophila Genetics and Immunocytochemistry—GMR[3]-Dronc-WT, GMR-Dronc-C318S, and GMR-Dronc-E352A flies were generated by constructing wild-type (WT) Dronc, Dronc-C318S, and Dronc-E352A into the glass multiple reporter (GMR) P element vector and then introducing these constructs into the *Drosophila* germline using standard techniques. GMR-Hid, GMR-Reaper, and GMR-Grim were generated as described (29). Multiple lines were generated. Consistently, GMR-Dronc-E352A and GMR-Dronc-C318S showed alleviated ablated eye phenotype when compared with those of GMR-Dronc-WT flies. Anti-Dronc antibody staining was carried out on third instar eye discs from flies of various genotypes essentially as described (29).

Analytical Ultracentrifugation—Protein samples were prepared in 25 mM phosphate-buffered saline with pH 8.0 and 150 mM NaCl. All sedimentation equilibrium experiments were performed with a Beckman Optima XL-I at the Center for Analytical Ultracentrifugation of Macromolecular Assemblies (the University of Texas Health Science Center at San Antonio, Department of Biochemistry). See supplemental data for details.

RESULTS

Dronc Undergoes Autocatalytic Cleavage—To understand how Dronc is activated, we reconstituted an *in vitro* activation assay for Dronc. The full-length WT Dronc was expressed in *E. coli* and purified to homogeneity (Fig. 1*A*, *lane 1*). The purification procedures for Dronc were carried out at 4 °C so as to maintain the WT Dronc protein in its zymogen form. When the single-chain WT Dronc zymogen was incubated at 22 °C, autocatalytic cleavage at a slow yet detectable rate was observed as evidenced by the initial appearance of two bands below the zymogen (Fig. 1*A*, *lanes 2–4*). Further autocatalytic cleavage resulted in the generation of two additional products (Fig. 1*A*, *lanes 5–7*).

Analysis of the initial cleavage products by N-terminal peptide sequencing identified the primary autocatalytic cleavage site to be after residue Glu^{352}, which is the last amino acid of a canonical Dronc substrate sequence Thr^{349}-Gln^{350}-Thr^{351}-Glu^{352} (^{349}TQTE^{352}). Although Dronc contains two putative caspase cleavage sites ^{110}DESD^{113} and ^{132}DIVD^{135} between its prodomain and the caspase unit, subsequent analysis by N-terminal peptide sequencing revealed that the additional cleavage products were due to a secondary cleavage site after residue Glu^{143} following an ^{140}EASE^{143} sequence. This observation is consistent with the finding that Dronc, in contrast to all other known caspases, prefers substrate specificity of Glu at the P1 position (30). The accelerated cleavage of Dronc was not due to other contaminating protease(s) because no cleavage was observed for the catalytically inactive Dronc (C318A) even after prolonged incubation (Fig. 1*A*, *lanes 8–9*).

Our studies indicated that the maturation of Dronc has two sequential cleavage events. The first and primary cleavage after Glu^{352} results in the separation of the caspase small subunit from the caspase large subunit and the prodomain, whereas the second cleavage after Glu^{143} removes the prodomain from the catalytic core domain. The first cleavage after Glu^{352} is required for the second cleavage after Glu^{143} because the mutant Dronc E352A, which eliminated the first cleavage site but contained WT catalytic residues, remained as a single polypeptide even after prolonged incubation (Fig. 1*A*, *lanes 10–11*).

To further characterize the autocatalytic cleavage, we incubated the catalytically inactive Dronc C318A zymogen, which contains Glu^{352}, with Dronc E352A, which contains WT catalytic residues but was unable to cleave itself due to the mutation E352A. The Dronc C318A zymogen was cleaved after Glu^{352}, resulting in two fragments (Fig. 1*B*). This result indicates that the autocatalytic cleavage of Dronc can occur in *trans* and further demonstrates that the mutant Dronc E352A is catalytically active, albeit the level of activity remains at the basal level (Fig. 1*B*).

Mature Dronc Exhibits Drastically Elevated Catalytic Activity—The autocatalytic cleavage of Dronc likely induces its activation. To confirm this conjecture, we reconstituted an *in vitro* Dronc activity assay to compare the catalytic activity of Dronc zymogen with that of the mature Dronc (Fig. 1*C*). The catalytically inactive Drice zymogen (residues 1–339, C196A) was used as a physiologically relevant substrate for Dronc. The fact that Dronc zymogen undergoes a process of autocleavage (Fig. 1*A*) potentially complicates the interpretation of results as the processed Dronc is expected to exhibit an elevated level of catalytic activity. To alleviate this problem, we used the uncleavable but catalytically active Dronc variant E352A as a WT zymogen substitute. Although the Dronc E352A zymogen exhibited a very low level of catalytic activity (Fig. 1*C*, *left panel*), the mature Dronc cleaved 90% of the

[3] The abbreviations used are: GMR, glass multiple reporter; WT, wild-type.

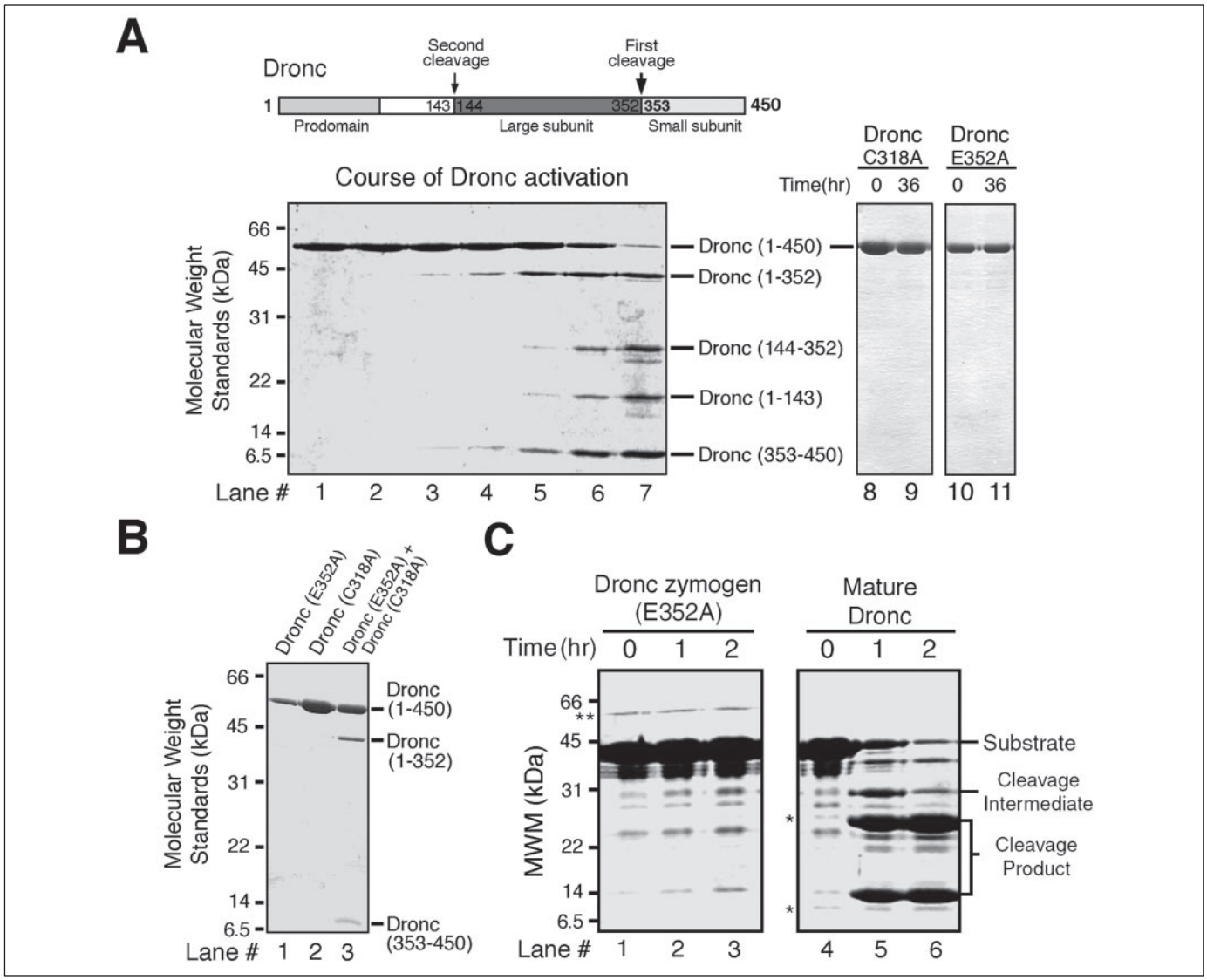

FIGURE 1. **The Dronc zymogen undergoes autocatalytic cleavage and subsequently exhibits a drastically enhanced level of catalytic activity.** *A*, the Dronc zymogen undergoes autocatalytic cleavages. A time course of Dronc autocatalytic cleavage was visualized by SDS-PAGE followed by Coomassie Blue staining. The cleavage products were identified by mass spectrometry and N-terminal peptide sequencing. *B*, the autocatalytic cleavage can occur in *trans*. Although neither Dronc E352A (*lane 1*) nor Dronc C318 (*lane 2*) was capable of autocatalytic cleavage, Dronc E352A cleaved Dronc C318A into two fragments following Glu^{352} (*lane 3*). The SDS-PAGE gel was stained by Coomassie Blue. *C*, mature Dronc exhibits a significantly elevated level of catalytic activity. A time course of Dronc activity was visualized by SDS-PAGE followed by Coomassie Blue staining. Catalytically inactive Drice zymogen was used as the substrate. An equimolar amount of Dronc zymogen (indicated by *double asterisks*) or mature Dronc (indicated by the *single asterisk*) was incubated with the substrate. Molecular weight markers (MWM) are indicated to the *left*.

substrate within the first hour of incubation (Fig. 1*C*, *right panel*). These experiments were performed under a condition that resembles the physiological pH and ionic strength (see "Experimental Procedures" for details). Similar results were obtained under other conditions (data not shown). Thus the autocleaved Dronc exhibits a catalytic activity that is drastically elevated over the zymogen.

Autocatalytic Cleavage of Dronc Shifts a Monomer into a Dimer—Although Dronc is the functional ortholog of mammalian caspase-9, our biochemical characterization demonstrates that they exhibit quite different patterns of activation. The prodomain of caspase-9 is required for the formation of an apoptosome holoenzyme, in which the activity of caspase-9 is allosterically regulated by Apaf-1 (8). Necessitated by this function, there is no caspase cleavage site between the prodomain and the caspase unit of caspase-9. Consequently, the prodomain and the large subunit of caspase-9 are a single polypeptide chain. In contrast, Dronc contains multiple caspase cleavage sites between its prodomain and the caspase unit, and the prodomain of Dronc is removed after a second autocatalytic cleavage event (Fig. 1*A*). These observations strongly suggest that, in contrast to activated caspase-9 as a holoenzyme, the mature Dronc protein may exist as a free enzyme. These observations further imply that Dronc may utilize a different mechanism for its activation.

To investigate the activation mechanism for Dronc, we first asked why the Dronc zymogen exhibited an extremely low level of catalytic activity through examination of the basal state of Dronc zymogen using gel filtration. Interestingly, the elution volume of the Dronc zymogen (residues 1–450, C318A) corresponded to an apparent molecular mass of ~50 kDa, consistent with that of a Dronc monomer (Fig. 2*A*, *solid line*). This observation suggests an explanation as to why the Dronc zymogen is marginally active since an unassisted caspase monomer is thought to be catalytically inactive due to the unproductive conformation of the active site (2).

Next, we examined the basal state of the autocleaved Dronc. Surprisingly, the elution of the cleaved Dronc (residues 1–352 and 353–450,

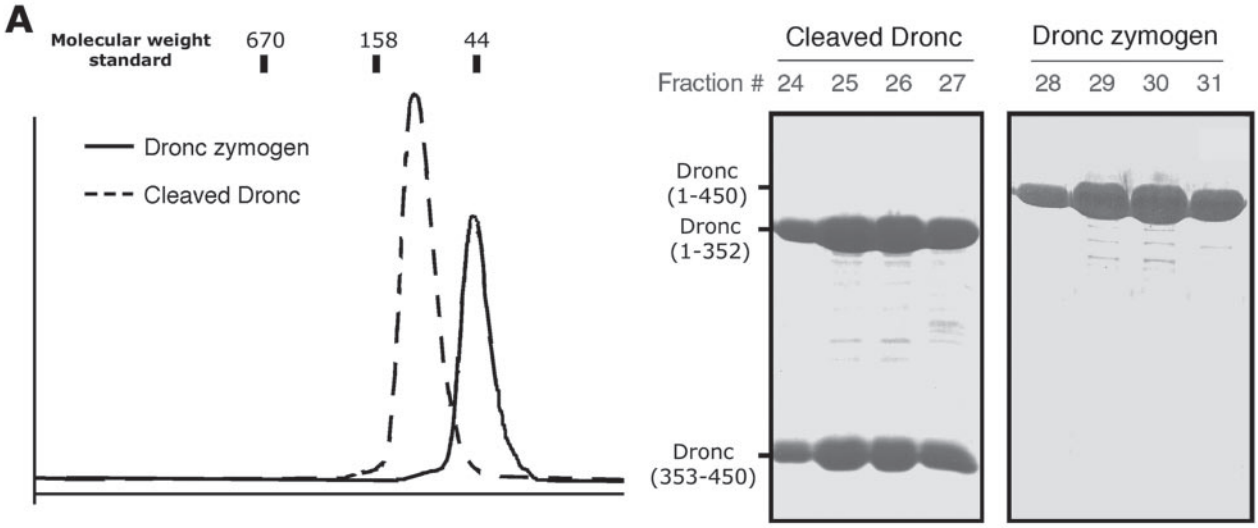

B

A summary of the analytical ultracentrifugation measurements

Sample	Model fitting	Observed monomer MW	Calculated monomer MW
Dronc zymogen	Monomer	34.8 ± 0.3 kDa	36.5 kDa
Cleaved Dronc	Monomer-dimer	Kd = 0.27 μM	

FIGURE 2. **Autocleavage of Dronc shifts a constitutive monomer into a stable dimer.** *A*, the Dronc zymogen appeared to be a monomer, but the autocleaved Dronc was primarily a dimer. Shown here is a superposition of the gel filtration chromatograms for the Dronc zymogen (*solid line*) and the autocleaved Dronc (*dashed line*). Both Dronc protein samples contained a mutation C318A on the catalytic residue Cys^{318} so as to eliminate a potential problem of protein degradation. The autocleaved Dronc was obtained by co-expression of the large (residues 1–352) and small (residues 353–450) subunits. Peak fractions were visualized by SDS-PAGE followed by Coomassie Blue staining (*right panels*). *B*, the Dronc zymogen exists exclusively as a monomer, but the autocleaved Dronc is primarily a dimer with a dissociation constant of 0.27 μM. These results were obtained from the analytical ultracentrifugation experiments (see Supplemental data). *MW*, molecular weight.

C318A) was shifted to earlier fractions (Fig. 2*A*, *dotted line*), with the elution volume corresponding to an apparent molecular mass of ~100 kDa. This observation strongly suggests that the primary autocatalytic cleavage induces the formation of a stable Dronc homodimer. To definitively confirm this finding, we performed analytical ultracentrifugation experiments (Fig. 2*B* and Supplemental data). As anticipated, the single-chain Dronc zymogen (residues 136–450, C318A) existed exclusively as a monomer in solution, with a fitted molecular mass of 34.8 + 0.3 kDa. In contrast, the two-chain Dronc (residues 136–352 and 353–450, C318A) existed primarily as a stable homodimer in solution, with a dissociation constant (K_d) of ~0.27 μM. Thus Dronc activation appears to employ an interesting mechanism; the cleavage after Glu^{352} triggers the transition from an inactive monomer for the Dronc zymogen to a catalytically active dimer for the cleaved Dronc.

Structure of Dronc Zymogen Reveals an Unproductive Conformation in the Active Site—To elucidate the molecular mechanism by which Dronc zymogen remains catalytically inactive, we expressed, purified, and crystallized a prodomain-deleted Dronc zymogen (residues 136–450, C318A). The structure was determined by multiwavelength anomalous dispersion and refined to 2.5 Å resolution (Table 1 and Fig. 3*A*). Each asymmetric unit contains one monomer of the Dronc zymogen.

Similar to other known caspases, the Dronc zymogen contains a central six-stranded β sheet, flanked on each side by three α helices (Fig. 3, *B* and *C*). In contrast to other caspases, the Dronc zymogen exhibits a number of unique structural features. For example, a 39-residue fragment (residues 158–196) at the N terminus forms an extended and rigid surface loop that zigzags across one side of the zymogen (Fig. 3, *A* and *B*). The fact that autocleavage after Glu^{352} leads to formation of a Dronc dimer suggests two possibilities; either the L2 loop interferes with dimer formation in the zymogen, or the cleaved L2 loop significantly strengthens dimer formation in the processed Dronc. In the crystals, the bulk of the L2 loop is disordered and does not allow a direct examination of the first possibility.

Four surface loops, L1, L2, L3, and L4, emanate from the structural core, forming a potential active site (Fig. 3*B*). The L2 loop appears to be highly flexible as the electron density after residue Ala^{318} becomes discontinuous. Loops L3 and L4 also exhibit some flexibility, as judged by their high temperature factors in the crystals. These structural observations are not surprising because these surface loops are completely exposed to solvent. Previous studies on caspase-7 showed that the active site loops only become ordered upon activation cleavage and binding to substrate or inhibitors (4).

Structural analysis reveals that the active site of the Dronc zymogen exists in an unproductive conformation (Fig. 3*D*). In contrast to the active site conformation of the activated, inhibitor-free caspase-7 (Fig.

TABLE 1
Summary of crystallographic analysis

	Native (Dronc)	Peak (Se1)	Inflection (Se2)	Remote (Se3)
Data sets				
Beamline	CHESS-A1	CHESS-F2	CHESS-F2	CHESS-F2
Space group	$I4_132$	$I4_132$	$I4_132$	$I4_132$
Wavelength (Å)	1.1000	0.9793	0.9791	0.964
Resolution (Å)	99–2.5	99–3.1	99–3.1	99–3.1
Unique reflections	12,899	6,540	6,534	6,553
Completeness (%) (outer shell)	99.7 (100.0)	94.4 (96.7)	94.5 (97.0)	94.6 (96.9)
R_{sym} [a] (outer shell)	0.055 (0.33)	0.107 (0.43)	0.093 (0.40)	0.097 (0.42)
Data redundancy	26.0	19.2	19.4	19.4
Average I/σ anomalous difference (%)	61.4 (15.6)	30.7 (8.9)	32.1 (9.1)	31.3 (8.9)
Refinement statistics				
Resolution range (Å)	20–2.5			
Number of reflections ($\|F\| > 0$)	12,855			
Total number of atoms (water)	2,228 (201)			
Completeness of data	99.6%			
R-factor[b] (*R*-free)	0.269 (0.222)			
r.m.s.d.[c]				
Bond (Å)	0.006			
Angle (deg.)	1.43			
Ramachandran plot				
Most favored	82.5%			
Additionally allowed	16.9%			
Generously allowed	0.5%			
Disallowed	0.0%			

[a] $R_{sym} = \Sigma_h\Sigma_i|I_{h,i} - I_h|/\Sigma_h\Sigma_i I_{h,i}$, where I_h is the mean intensity of the *i* observations of symmetry-related reflections of *h*.
[b] $R = \Sigma|F_{obs} - F_{calc}|/\Sigma F_{obs}$, where $F_{obs} = F^P$, and F_{calc} is the calculated protein structure factor from the atomic model (R_{free} was calculated with 5% of the reflections).
[c] r.m.s.d. (root-mean-square deviation) in bond lengths and angles are the deviations from ideal values.

3, *D* and *E*) or the activated, inhibitor-bound caspase-9 (Fig. 3*F*), the substrate-binding groove in Dronc zymogen is absent in this conformation. Previous studies showed that, to form a productive active site conformation for a caspase, the L2 loop, which contains the catalytic residue, must interact with other structural elements such as the L2′ loop from the adjacent monomer (Fig. 3, *E* and *F*). However, the monomeric Dronc zymogen lacks such supporting elements from an adjacent monomer. These structural features do not support substrate binding or catalysis and are consistent with the biochemical observation that the Dronc zymogen remains catalytically inactive.

Uncleavable Dronc Zymogen Is Dominant Negative in Vivo—Our biochemical characterization demonstrates that the Dronc zymogen is constitutively monomeric in solution and catalytically inactive due to an unproductive conformation at the active site. The autocleavage after Glu^{352} favors the formation of a Dronc dimer, which presumably results in the alteration of the unproductive active site conformation. *In vivo*, the autoactivation process of Dronc is likely facilitated by Dark/Hac-1/Dapaf-1 as Dronc activation in *Drosophila* cells requires Dark/Hac-1/Dapaf-1 (19–21). These analyses predict that an uncleavable Dronc zymogen E352A will likely act in a dominant negative fashion *in vivo* as this protein may compete with WT Dronc zymogen for binding to Dark/Hac-1/Dapaf-1.

To corroborate our biochemical and structural findings, we generated transgenic flies overexpressing the WT Dronc, the catalytic mutant Dronc (C318S), or the uncleavable Dronc (E352A) under the eye-specific GMR promoter. Indeed, although overexpression of the WT Dronc caused an ablated eye phenotype (Fig. 4*A*), overexpression of the catalytic mutant Dronc (Fig. 4*B*) or the uncleavable Dronc (Fig. 4*C*) had little impact on the eyes, suggesting that these Dronc variants were unable to become activated *in vivo*. The pro-apoptotic proteins Reaper, Hid, and Grim (RHG) function by antagonizing the activity of DIAP1 (31). Overexpression of the pro-apoptotic genes Reaper, Grim, and Hid led to induction of cell death and ablated eye phenotypes (Fig. 4, *D–F*). Coexpression of the Dronc catalytic mutant (C318S) (Fig. 4, *G–I*) or the uncleavable Dronc (E352A) (Fig. 4, *J–L*) partially suppressed the ablated eye phenotype. In *Drosophila*, continuous activity of Dark/Hac-1/Dapaf-1 is required for normal apoptosis (32). Presumably, the catalytically inactive Dronc zymogen or the uncleavable Dronc was able to bind to and saturate all available Dark/Hac-1/Dapaf-1 protein and thus had a negative impact on the autoactivation of WT Dronc protein mediated by Dark/Hac-1/Dapaf-1.

DISCUSSION

Previous studies on the activation of mammalian initiator caspases have revealed significant insights into the mechanisms. Zymogen of both caspase-8 and caspase-2 was found to exist mainly as a monomer by gel filtration (13–15). In contrast, the autocleaved wild-type caspase-8 exists in an equilibrium between monomers and dimers, with a dissociation constant of ~50 μM (14). The processed wild-type caspase-2 also preferentially formed homodimers (15). These findings strongly argue that dimerization is a crucial factor for the activation of caspase-8 and caspase-2 and that the autocatalytic cleavage in these mammalian initiator caspases plays an important role for their activation.

In this study, we investigate the activation mechanism for the *Drosophila* initiator caspase Dronc. We demonstrate that the Dronc zymogen exists exclusively as a monomer in solution and forms a stable dimer following the primary autocatalytic cleavage after Glu^{352}. A cleavage mutant Dronc (E352A) does not undergo autocatalytic cleavage and remains a monomer in solution. The structure of the Dronc zymogen, representing the first structure of an uncleaved initiator caspase zymogen, reveals an unproductive active site conformation. At present, we do not yet have a structure of the activated, dimeric Dronc, which is expected to reveal the precise conformation of the active site. Nonetheless, previous studies on dimeric caspases suggest that the active site of one Dronc monomer is likely stabilized by the adjacent monomer through the provision of a critical surface loop (L2′) (33). Our results demonstrate that the autocatalytic cleavage after Glu^{352} of Dronc greatly facilitates its dimerization, which is essential for its catalytic activity.

If Dronc zymogen exists exclusively as a monomer in solution, how can autocatalytic cleavage occur? There are two possibilities. One is that

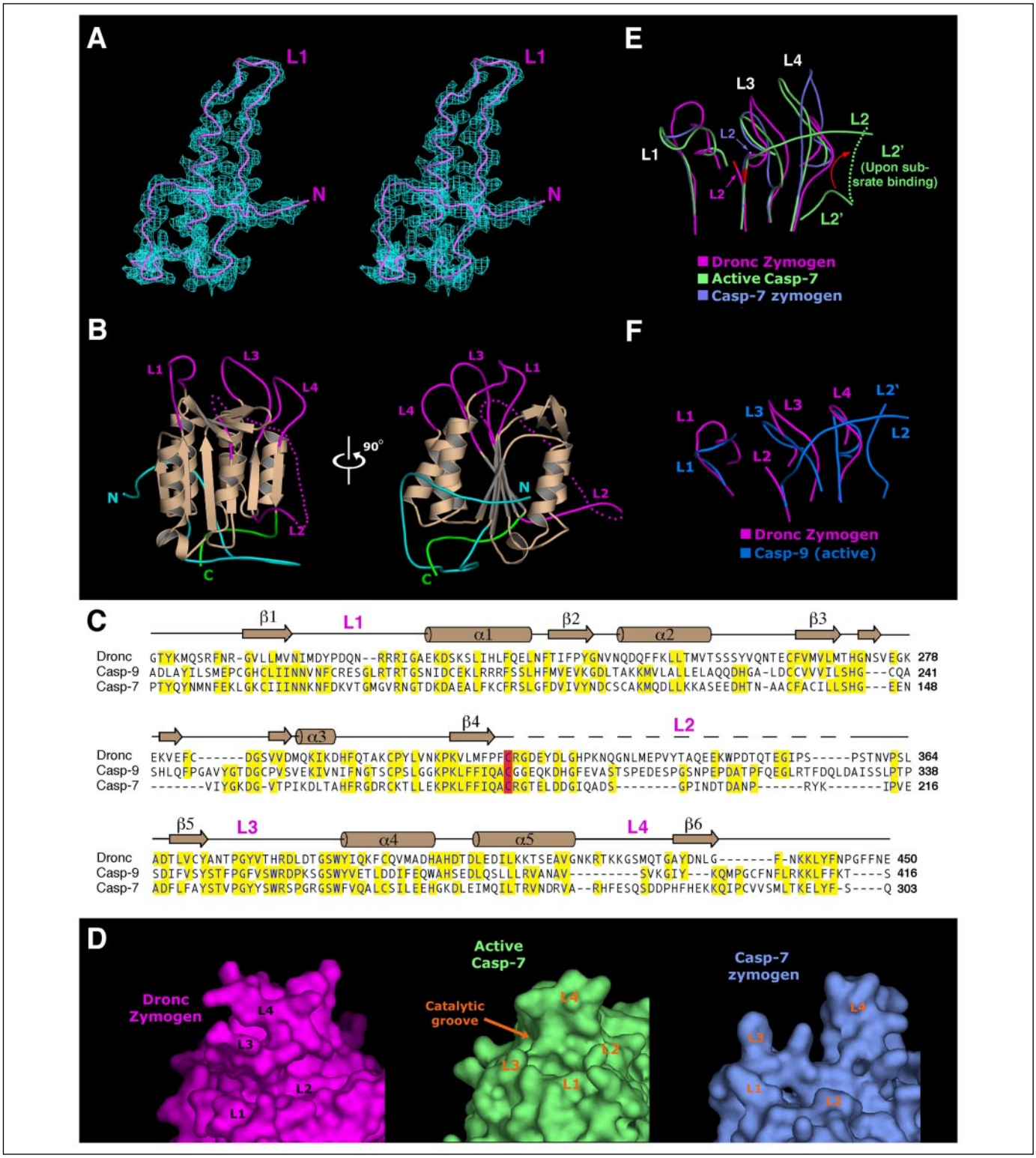

FIGURE 3. **Structure of the Dronc zymogen reveals a molecular basis for the lack of catalytic activity.** *A*, a representative portion of the electron density $2F_o - F_c$ map, contoured at 1.1 σ and colored *cyan*, was shown in stereo around amino acid residues 158–230. *B*, overall structure of the Dronc zymogen in two perpendicular views. The structural core of Dronc zymogen is shown in *brown*, with the active site loops highlighted in *magenta*. The extended N-terminal fragment (residues 158–196) is colored *cyan*. The four loops defining the potential catalytic site are *labeled*. *C*, sequence alignment among Dronc, caspase-9 (*Casp-9*), and caspase-7 (*Casp-7*). Because the N-terminal fragment of Dronc exhibits no apparent sequence similarity with caspase-9 or caspase-7, only residues 185–450 of Dronc are shown here. The secondary structural elements of the Dronc zymogen are indicated above the sequences. Conserved residues are colored *yellow*. *D*, the appropriate substrate-binding groove is absent in the Dronc zymogen. When compared with the activated, inhibitor-free caspase-7 (*middle panel*), the Dronc zymogen does not have an appropriate substrate-binding groove (*left panel*). The active site of the caspase-7 zymogen is shown here as a control (*right panel*). *E*, comparison of the conformations of the active site loops among Dronc zymogen, the activated inhibitor-free caspase-7, and the caspase-7 zymogen. The *green dotted line* represents the L2′ loop in the activated inhibitor-bound caspase-7. *F*, the active site conformation of the Dronc zymogen is quite different from that of the inhibitor-bound caspase-9 (inhibitor omitted for clarity). The active site conformation of caspase-9 is critically supported by the L2′ loop, which is provided by the adjacent monomer. However, in Dronc zymogen, the monomeric and uncleaved nature prevents the provision of the L2′ loop.

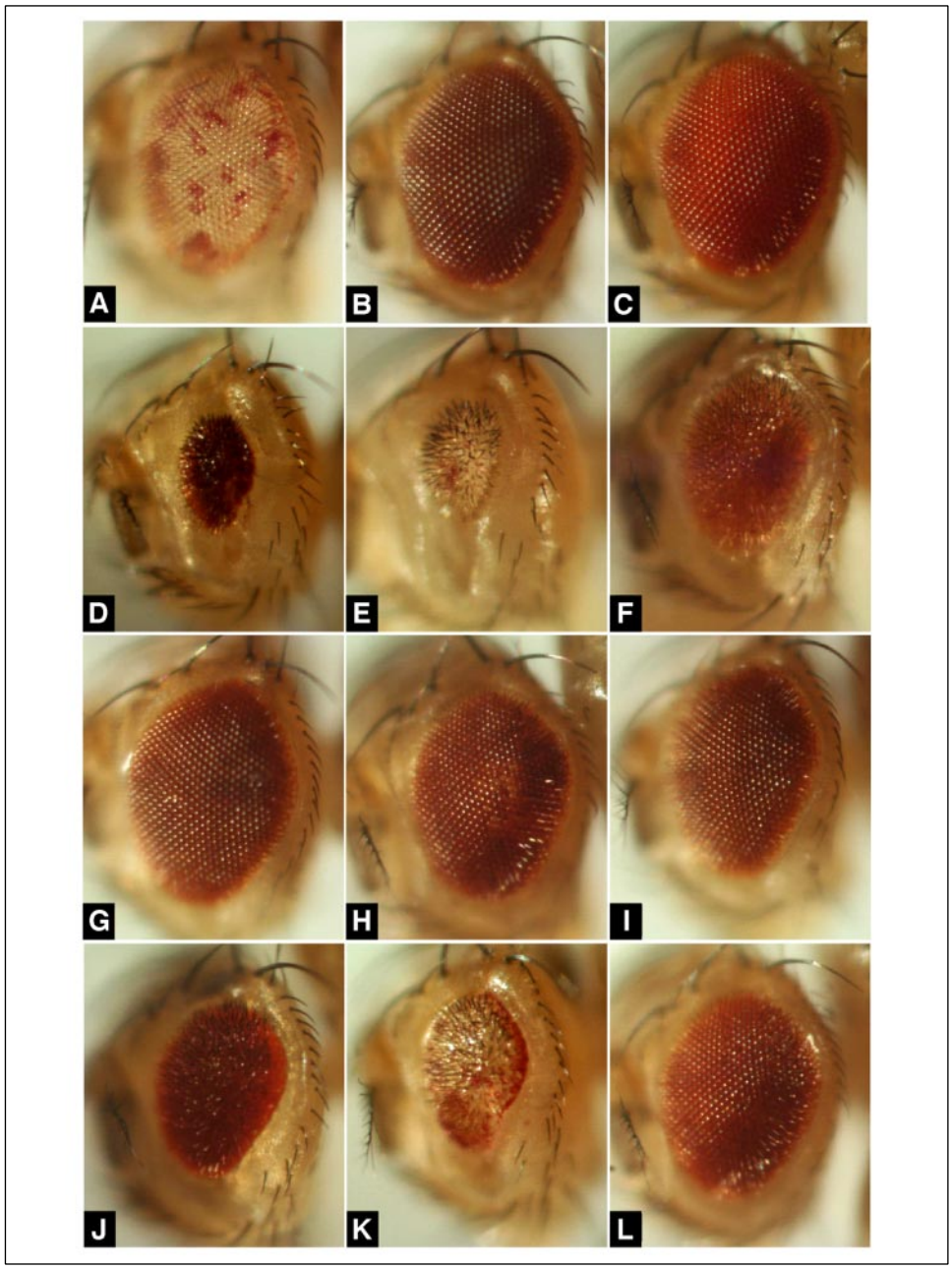

FIGURE 4. **Uncleavable Dronc zymogen is dominant negative *in vivo*.** Genotypes are as follows: GMR-Dronc/+ (*A*), GMR-Dronc-C318S/+ (*B*), GMR-Dronc-E352A/+ (*C*), GMR-Rpr/+ (*D*), GMR-Grim/+ (*E*), GMR-Hid/+ (*F*), GMR-Rpr/GMR-Dronc-C318S (*G*), GMR-Grim/GMR-Dronc-C318S (*H*), GMR-Hid/GMR-Dronc-C318S (*I*), GMR-Rpr/GMR-Dronc-E352A (*J*), GMR-Grim/GMR-Dronc-E352A (*K*), and GMR-Hid/GMR-Dronc-E352A (*L*).

the monomeric zymogen can associate transiently into dimers, as suggested for the initiator caspase-2 (15). Then the transiently dimerized Dronc zymogens process each other in *trans*. The other possibility is that the monomeric Dronc zymogen can exhibit a very low level of catalytic activity for its own intramolecular cleavage. Although our current study does not allow differentiation of these two scenarios, the experimental evidence indicated that the autocatalytic cleavage of Dronc can occur in *trans*, suggesting that the cleavage might be a result of transient dimerization. However, our data are merely suggestive, and we do not know whether the autocatalytic cleavage can also occur intramolecularly. Nonetheless, our results unambiguously show that the autocatalytic cleavage greatly facilitates the formation of a homodimer for Dronc.

Although Dronc is the functional homolog of the mammalian caspase-9, their activation mechanisms appear to be quite different (Fig. 5). For caspase-9, the intrachain cleavage is not necessary for its activation as the fully processed caspase-9 in isolation is only marginally active, much the same way as the unprocessed caspase-9 zymogen (8, 10, 34). Rather, association with the apoptosome leads to a dramatic increase (up to 2000-fold) for the catalytic activity of the processed as well as the unprocessed caspase-9 (8, 10). Necessitated by association with apoptosome, the prodomain of caspase-9 remains covalently linked to the large subunit of the caspase unit. In contrast to caspase-9, the free, processed Dronc exhibits a catalytic activity that is several orders of magnitude higher than the Dronc zymogen (Fig. 1*C*). The extent of activity improvement is reminiscent of catalytic activation for other caspases (35). Thus the processed, free Dronc likely represents the fully activated state. This notion is supported by the observation that the prodomain of Dronc, which is responsible for binding to Dark/Hac-1/Dapaf-1, is removed from the caspase unit in the mature enzyme. In addition, the presence of recombinant Dark/Hac-1/Dapaf-1 protein does not enhance the catalytic activity of the mature Dronc.[2]

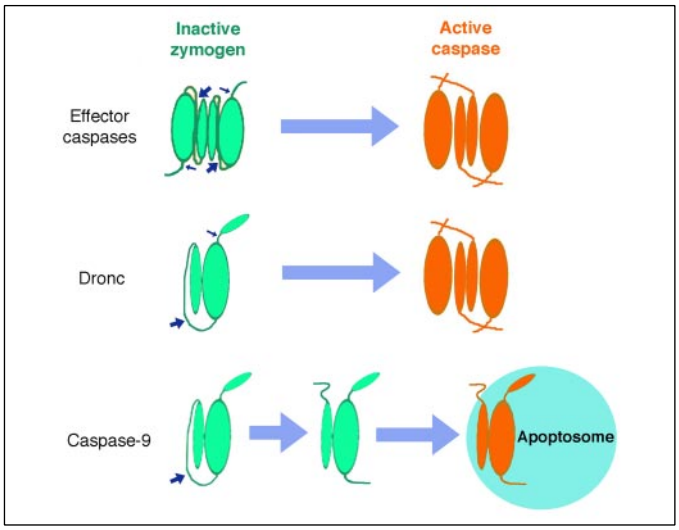

FIGURE 5. **A comparison of Dronc activation with activation of other caspases.** This comparison reveals that Dronc exhibits features of both initiator and effector caspases. The inactive zymogens and the activated caspases are colored *green* and *orange*, respectively. The *thick* and *thin arrows* denote the primary and secondary cleavage events, respectively.

Isolated caspase-9 exists constitutively as a monomer in solution, both in its zymogen state and in the autocleaved form (9) (Fig. 5). Caspase-3 or caspase-7, on the other hand, exists constitutively as a homodimer in solution, both in its zymogen form and in the cleaved, activated state (Fig. 5). In contrast to both caspase-9 and caspase-3, Dronc exists exclusively as a monomer in the zymogen state and forms a stable dimer with a dissociation constant of 0.27 μM following the primary autocatalytic cleavage. The mammalian initiator caspases, caspase-8 and caspase-2, exhibit an increased preference for the formation of homodimer following the autocatalytic cleavage. In this regard, the activation of the initiator caspases, Dronc in *Drosophila* and caspase-8/-2 in mammals, incorporates a feature reminiscent of effector caspases (Fig. 5). In a more general sense, our study reveals another level of complexity in the activation of caspases and suggests diverse mechanisms for the activation of initiator caspases.

It should be pointed out that the model presented (Fig. 5) only highlights certain biochemical aspects of caspase activation. There are a number of other important considerations to caspase activation *in vivo*. For example, the activation of Dronc in *Drosophila* cells requires the presence of Dark/Hac-1/Dapaf-1 (19–21,32). A recent study showed that the Dark/Hac-1/Dapaf-1 protein forms a double-donut-shaped apoptosome, with each donut ring comprising eight molecules of Dark/Hac-1/Dapaf-1 (36). The Dark/Hac-1/Dapaf-1 apoptosome may greatly facilitate the recruitment and the activation of the Dronc zymogen by enhancing its dimerization. However, the mechanism by which the Dark/Hac-1/Dapaf-1 apoptosome activates the Dronc zymogen is likely to be different from that by which the Apaf-1 apoptosome activates caspase-9. The detailed activation mechanisms for initiator caspases remain to be investigated by biochemistry and structural biology.

Acknowledgments—We thank Lana Walsh for beam time at CHESS and Michael Becker for beam time at Brookhaven National Laboratory. The development of the UltraScan Software is supported by the National Science Foundation through Grant DBI-9974819 to B. Demeler.

REFERENCES

1. Thornberry, N. A., and Lazebnik, Y. (1998) *Science* **281,** 1312–1316
2. Riedl, S. J., and Shi, Y. (2004) *Nat. Rev. Mol. Cell Biol.* **5,** 897–907
3. Budihardjo, I., Oliver, H., Lutter, M., Luo, X., and Wang, X. (1999) *Annu. Rev. Cell Dev. Biol.* **15,** 269–290
4. Chai, J., Wu, Q., Shiozaki, E., Srinivasula, S. M., Alnemri, E. S., and Shi, Y. (2001) *Cell* **107,** 399–407
5. Riedl, S. J., Fuentes-Prior, P., Renatus, M., Kairies, N., Krapp, S., Huber, R., Savesen, G. S., and Bode, W. (2001) *Proc. Natl. Acad. Sci. U. S. A.* **98,** 14790–14795
6. Shi, Y. (2004) *Cell* **117,** 855–858
7. Wang, X. (2001) *Genes Dev.* **15,** 2922–2933
8. Rodriguez, J., and Lazebnik, Y. (1999) *Genes Dev.* **13,** 3179–3184
9. Shiozaki, E. N., Chai, J., Rigotti, D. J., Riedl, S. J., Li, P., Srinivasula, S. M., Alnemri, E. S., Fairman, R., and Shi, Y. (2003) *Mol. Cell* **11,** 519–527
10. Srinivasula, S. M., Saleh, A., Hedge, R., Datta, P., Shiozaki, E., Chai, J., Robbins, P. D., Fernandes-Alnemri, T., Shi, Y., and Alnemri, E. S. (2001) *Nature* **409,** 112–116
11. Renatus, M., Stennicke, H. R., Scott, F. L., Liddington, R. C., and Salvesen, G. S. (2001) *Proc. Natl. Acad. Sci. U. S. A.* **98,** 14250–14255
12. Chao, Y., Shiozaki, E. N., Srinivasula, S. M., Rigotti, D. J., Fairman, R., and Shi, Y. (2005) *PLoS Biol.* **3,** e183
13. Boatright, K. M., Renatus, M., Scott, F. L., Sperandio, S., Shin, H., Pedersen, I. M., Ricci, J. E., Edris, W. A., Sutherlin, D. P., Green, D. R., and Salvesen, G. S. (2003) *Mol. Cell* **11,** 529–541
14. Donepudi, M., Mac Sweeney, A., Briand, C., and Grutter, M. G. (2003) *Mol. Cell* **11,** 543–549
15. Baliga, B. C., Read, S. H., and Kumar, S. (2004) *Cell Death Differ.* **11,** 1234–1241
16. Dorstyn, L., Colussi, P. A., Quinn, L. M., Richardson, H., and Kumar, S. (1999) *Proc. Natl. Acad. Sci. U. S. A.* **96,** 4307–4312
17. Chew, S. K., Akdemir, F., Chen, P., Lu, W. J., Mills, K., Daish, T., Kumar, S., Rodriguez, A., and Abrams, J. M. (2004) *Dev. Cell* **7,** 897–907
18. Daish, T. J., Mills, K., and Kumar, S. (2004) *Dev. Cell* **7,** 909–915
19. Kanuka, H., Sawamoto, K., Inohara, N., Matsuno, K., Okano, H., and Miura, M. (1999) *Mol. Cell* **4,** 757–769
20. Zhou, L., Song, Z., Tittel, J., and Steller, H. (1999) *Mol. Cell* **4,** 745–755
21. Rodriguez, A., Oliver, H., Zou, H., Chen, P., Wang, X., and Abrams, J. M. (1999) *Nat. Cell Biol.* **1,** 272–279
22. Muro, I., Monser, K., and Clem, R. J. (2004) *J. Cell Sci.* **117,** 5035–5041
23. Yan, N., Wu, J.-W., Huh, J. R., Chai, J., Li, W., Hay, B. A., and Shi, Y. (2004) *Nat. Struct. Mol. Biol.* **11,** 420–428
24. Otwinowski, Z., and Minor, W. (1997) *Methods Enzymol.* **276,** 307–326
25. Terwilliger, T. C., and Berendzen, J. (1999) *Acta Crystallogr. Sect. D Biol. Crystallogr.* **55,** 849–861
26. Collaborative Computational Project, N. (1994) *Acta Crystallogr. Sect. D Biol. Crystallogr.* **50,** 760–763
27. Jones, T. A., Zou, J.-Y., Cowan, S. W., and Kjeldgaard, M. (1991) *Acta Crystallogr. Sect. A* **47,** 110–119
28. Brunger, A. T., Adams, P. D., Clore, G. M., Delano, W. L., Gros, P., Grosse-Kunstleve, R. W., Jiang, J. S., Kuszewski, J., Nilges, M., Pannu, N. S., Read, R. J., Rice, L. M., Simonson, T., and Warren, G. L. (1998) *Acta Crystallogr. Sect. D Biol. Crystallogr.* **54,** 905–921
29. Yoo, S. J., Huh, J. R., Muro, I., Yu, H., Wang, L., Wang, S. L., Feldman, R. M., Clem, R. J., Muller, H. A., and Hay, B. A. (2002) *Nat. Cell Biol.* **4,** 416–424
30. Hawkins, C. J., Yoo, S. J., Peterson, E. P., Wang, S. L., Vernooy, S. Y., and Hay, B. A. (2000) *J. Biol. Chem.* **275,** 27084–27093
31. Hay, B. A., Huh, J. R., and Guo, M. (2004) *Nat. Rev. Genet.* **5,** 911–922
32. Rodriguez, A., Chen, P., Oliver, H., and Abrams, J. M. (2002) *EMBO J.* **21,** 2189–2197
33. Shi, Y. (2002) *Mol. Cell* **9,** 459–470
34. Stennicke, H. R., Deveraux, Q. L., Humke, E. W., Reed, J. C., Dixit, V. M., and Salvesen, G. S. (1999) *J. Biol. Chem.* **274,** 8359–8362
35. Salvesen, G. S., and Dixit, V. M. (1999) *Proc. Natl. Acad. Sci. U. S. A.* **96,** 10964–10967
36. Yu, X., Wang, L., Acehan, D., Wang, X., and Akey, C. (2006) *J. Mol. Biol.* **355,** 577–589